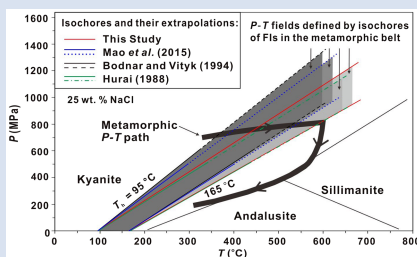# *In situ* determination of NaCl-H$_2$O isochores up to 900 °C and 1.2 GPa in a hydrothermal diamond-anvil cell

## J.K. Li[1*], I-M. Chou[2*], X. Wang[1,3]

OPEN ACCESS

## Abstract

https://doi.org/10.7185/geochemlet.2429



NaCl-H$_2$O is a typical binary system solution in geologic environments. However, its available *PVTX* properties (*e.g.*, isochores) are primarily applicable in the pressure-temperature (*P–T*) range of <600 MPa and <700 °C. Here, we performed 53 experiments in a hydrothermal diamond-anvil cell (HDAC) to determine NaCl-H$_2$O isochores by using the newly defined α-β quartz *P–T* transition boundary as a pressure calibrant (Li and Chou, 2022). The refined isochores fitted with our data are expressed by: $P\,(bar) = A_1 + A_2 \times T\;(°C)$ and

$$A_1 = 0.0061 + (0.2385 - a_1) \times T_h - (0.002855 + a_2) \times T_h^2 - (a_3 \times T_h + a_4 \times T_h^2) \times m$$

$$A_2 = a_1 + a_2 \times T_h + 9.888 \times 10^{-6} \times T_h^2 + (a_3 + a_4 \times T_h) \times m$$

where $m$ is the NaCl molality (mole/kg H$_2$O), $T_h$ (°C) is the liquid-vapour homogenisation (to the liquid phase) temperature, and $a_1$, $a_2$, $a_3$, and $a_4$ are constants (27.21, −0.05956, −0.3095, and 0.003232, respectively). The isochores have better applicability for the salinity range of 5−25 wt. % NaCl, 100 °C < $T_h$ <450 °C, and *P–T* range up to ~1.2 GPa and ~900 °C. Compared with previous data, these isochores are more precise above 600 MPa, and are particularly suitable for the geological applications involving saline fluids in the deep Earth.

## Introduction

NaCl-H$_2$O solutions exist widely in geologic environments. The properties of the pressure, volume, temperature, and composition (*PVTX*) of the binary system have been widely investigated to interpret the rock- and ore-forming conditions, and quantify mass transfer in many geological settings, such as subduction zones (Mantegazzi *et al.*, 2013). Empirical and theoretical models have been published to describe the *PVTX* properties of NaCl-H$_2$O (*e.g.*, Bodnar and Vityk, 1994). However, most *PVTX* models for NaCl-H$_2$O are applicable under low temperature (*e.g.*, ≤700 °C) and pressure (*e.g.*, ≤600 MPa) conditions (*e.g.*, Bodnar and Sterner, 1987; Mao *et al.*, 2015). This is mainly because these *PVTX* properties were derived from experimental results, such as those obtained with synthetic fluid inclusion (SFI) methods, using pressure vessels operated under relatively low *P–T* conditions (Gehrig, 1980; Zhang and Frantz, 1987; Bodnar and Vityk, 1994). Moreover, many *PVTX* models were built by using the equation of state (EoS) of H$_2$O suggested by Haar *et al.* (1984) (*e.g.*, Driesner, 2007), which has been considered to have lower accuracy than other available models at pressures >600 MPa (*e.g.*, Li and Chou, 2022). Consequently, most current available EoSs of H$_2$O-NaCl are only applicable to the upper crustal *P–T* conditions and thus unsuitable for describing geological processes in lower crustal conditions, such as those

involving the saline aqueous fluids released from subduction slabs where the pressure may become much higher than 600 MPa (*e.g.*, Kawamoto *et al.*, 2018).

In order to experimentally model such high *P–T* conditions, the hydrothermal diamond-anvil cell (HDAC; Bassett *et al.*, 1993), is a good option. It can potentially yield a sample chamber with a constant volume during an experiment at pressures up to 2.5 GPa and temperatures from −190 °C to 1200 °C (Bassett *et al.*, 1993), making it excellent to measure the *PVTX* properties or isochores of fluids under wide *P–T* conditions. By using the HDAC to measure the *PVTX* properties of a fluid, it is crucial to determine the pressure value at a set temperature in a homogenous fluid phase inside the sample chamber (Figure S-1a). Previously, pressure sensors based on shifts of Raman or fluorescence lines in some minerals or materials (*e.g.*, quartz and ruby) were commonly used in HDAC experiments, despite their large associated uncertainties (Schmidt and Ziemann, 2000). By using these pressure sensors, Mantegazzi *et al.* (2013) used a diamond-anvil cell to determine the *PVTX* properties of NaCl-H$_2$O solutions at 0.5–4.5 GPa and ≤400 °C (extrapolated up to 800 °C).

To obtain NaCl-H$_2$O isochore data with high precision in a wide *PVTX* range through HDAC experiments, this study uses the α-β quartz phase transition *P–T* boundary as the pressure calibrant (Figure S-1a), as done by Shen *et al.* (1993).

1. MNR Key Laboratory of Metallogeny and Mineral Assessment, Institute of Mineral Resources, Chinese Academy of Geological Sciences, Beijing 100037, China
2. CAS Key Laboratory of Experimental Study under Deep-sea Extreme Conditions, Institute of Deep-sea Science and Engineering, Chinese Academy of Sciences, Sanya, Hainan 572000, China
3. China University of Geosciences (Beijing), Beijing 100083, China
* Corresponding authors (email: Li9968@126.com, imchou@idsse.ac.cn)

In HDAC experiments, the α-β quartz phase transition temperature ($T_{tr}$) can be measured by optical observation of interference fringes (Shen *et al.*, 1993) or the Raman shifts of the quartz 464 cm$^{-1}$ band (Schmidt and Ziemann, 2000), with rigourous experimental conditions but large uncertainties (Li and Chou, 2022). Recently, Li and Chou (2022) found that the abrupt change in the Raman shift of the quartz 128 cm$^{-1}$ band is much more sensitive and precise than that of the 464 cm$^{-1}$ band during heating for the detection and measurement of the $T_{tr}$, particularly under high $P$ conditions (Figure S-1b); a new α-β quartz $P-T$ boundary with high precision was redefined by Li and Chou (2022). Moreover, a cooling system for HDAC was designed (Li *et al.*, 2020), which can be used to determine the true salinities of the loaded $H_2O$-NaCl solutions through ice melting temperatures ($T_{ice}$s). This prevents an erroneous assumption that the salinity of the prepared $H_2O$-NaCl solution is the true salinity of the loaded fluid, ignoring the effect of unavoidable evaporation of water and the corresponding increase in the salinity during loading (Li *et al.*, 2020). These new experimental procedures to measure the pressure and salinity can be applied to obtain fluid isochores with high precisions, especially at elevated temperatures and pressures. Therefore, here we loaded NaCl-$H_2O$ solutions in an HDAC sample chamber together with a chip of natural quartz (Figure S-2) to measure NaCl-$H_2O$ isochores with a Raman spectrometer.

## Experimental Results

Experimental details are provided in the Supplementary Information (Experimental Methods). A total of 53 experiments with $P-T$ range up to 1.2 GPa and 900 °C have been conducted with HDAC in this study. In each experiment, the $T_{ice}$, $T_{tr}$, and liquid–vapour homogenisation (to liquid phase) temperature ($T_h$) of the sample fluid were recorded (Table S-1). During heating, the Raman shifts of the 128 cm$^{-1}$ Raman band of α-quartz in the sample chamber were collected in each experiment to determine $T_{tr}$s (Figure S-1b). Subsequently, the α-β quartz phase transition pressure ($P_{tr}$) was calculated from $T_{tr}$ according to the refined α-β quartz $P-T$ boundary of Li and Chou (2022).

Each isochore of NaCl-$H_2O$ in our experiment is established through two $P-T$ points; one is the $P_h-T_h$ of the NaCl-$H_2O$ system in the HDAC sample chamber, and the other is $P_{tr}-T_{tr}$ described above (Figure S-1a). The $P_h$ is the liquid-vapour homogenisation (to the liquid phase) pressure for the sample NaCl-$H_2O$ fluid calculated from the measured $T_h$ by using the equation of Bodnar (1983). All the $P-T$ data of the NaCl-$H_2O$ isochores are presented in Table S-1 and Figure 1.

## Discussion

*Isochores fitted with the experimental data.* To facilitate the interpolation of our experimental results, we used the equation formats provided by Zhang and Frantz (1987) to fit the $H_2O$-NaCl isochores determined with ($T_h$, $P_h$) and ($T_{tr}$, $P_{tr}$) listed in Table S-1. This is because their equations were built with the liquid-vapour homogenisation $T$ and $P$ and the corresponding entrapment $P-T$ conditions of SFIs, which are similar to the data groups ($T_h$, $P_h$ and $T_{tr}$, $P_{tr}$) collected in this study (Table S-1). Moreover, their equations can accurately describe *PVTX* data from many experiments, as commented by Brown (1989). Accordingly, the $H_2O$-NaCl isochores of this study can be fitted by the following equation with $R^2 = 0.991$:

$$P\,(bar) = A_1 + A_2 \times T\,(°C) \qquad \text{Eq. 1}$$

where

$$A_1 = 0.0061 + (0.2385 - a_1) \times T_h - (0.002855 + a_2) \times T_h^2 \\ - (a_3 \times T_h + a_4 \times T_h^2) \times m$$

and

$$A_2 = a_1 + a_2 \times T_h + 9.888 \times 10^{-6} \times T_h^2 + (a_3 + a_4 \times T_h) \times m$$

The constants $A_1$ and $A_2$ are functions of $T_h$ (°C) of the fluid inclusions or NaCl-$H_2O$ solution in the HDAC sample chamber and salinity ($m$, the NaCl molality in aqueous solution). The parameters $a_1$, $a_2$, $a_3$, and $a_4$ are 27.21, −0.05956, −0.3095, and 0.003232, respectively. The average errors between the values calculated from Equation 1 and the experimental data for $P_{tr}$ and isochore slopes are 3.7 % and 3.9 %, respectively (Table S-1). These fitting errors among NaCl-$H_2O$ fluids with low to high salinities are consistent (Table S-1), and they are different from those of Zhang and Frantz (1987) which contain large errors for high density NaCl-$H_2O$ solutions, as pointed out by Brown (1989), indicating a better fitting of Equation 1 in this study. Considering the $P-T$ range of our experiments, Equation 1 is considered to have better applicability for solutions with salinity and $T_h$ ranges of 5−21 wt. % NaCl and 100−450 °C, respectively.

*Comparisons of experimental data with previous studies.* The experimental data of this study are compared with those derived from Bodnar and Vityk (1994) and Mao *et al.* (2015) (Figure 1). The model of Bodnar and Vityk (1994), determined using the SFI method, is applicable at ≤600 MPa, and has been widely used to interpret the *PVTX* properties of geological fluids (*e.g.*, Sullivan *et al.*, 2022). Mao's model (Mao *et al.*, 2015), as a representative thermodynamic model, works up to 1000 °C and 500 MPa. The agreements, among the $P_{tr}$ obtained from our experimental data and those from Bodnar and Vityk (1994) and Mao *et al.* (2015) below 600 MPa for the measured $T_{tr}$s (Figure 1), demonstrate the reliability of our experimental method and results. However, the deviations of $P_{tr}$ values obtained in our experiments from those extrapolated from the previous isochores, particularly Bodnar and Vityk (1994), are evident above 600 MPa, and they increase with salinity (Figure 1).

The isochores of NaCl-$H_2O$ solutions calculated with Equation 1 in this study were primarily compared with those derived from Hurai (1988), Bodnar and Vityk (1994), and Mao *et al.* (2015) in Figure 2. Note that the isochores of NaCl-$H_2O$ fluids in Bodnar and Vityk (1994) derived from the SFI technology were approximated by connecting the $P-T$ point at which the SFI was formed ($P_f-T_f$), and the $P-T$ point defined by the observed liquid-vapour homogenisation (to liquid phase) $T$ ($P_h-T_h$), assuming the volumes of the studied SFI at these two $P-T$ points were the same (isochoric) (Bodnar, 1995). However, it was clearly shown in Figure 17.3 of Bodnar and Sterner (1987) that, even for the pure $H_2O$ system, the volumes of the studied SFIs at these two $P-T$ points were not expected to be the same for most of SFIs (Bodnar and Sterner, 1987; their Table 17.1). To clearly demonstrate their warning, their experimental results for SFIs trapped at 100 MPa and 300, 400, 500 and 600 °C were shown in Figure S-3 by adding the isochores based on the densities of pure $H_2O$ at these two $P-T$ points, which were derived from the well established EoS of $H_2O$ IAPWS-95 (Wagner and Pruß, 2002). Therefore, the isochores obtained by SFI methods should strictly be called as iso-$T_h$ lines, unless the SFI volumes are corrected. Conversely, our isochores were measured *in situ*, during which the volume of the HDAC sample chamber was kept constant. Accordingly, the isochores of this study with high salinities and low $T_h$s evidently deviate
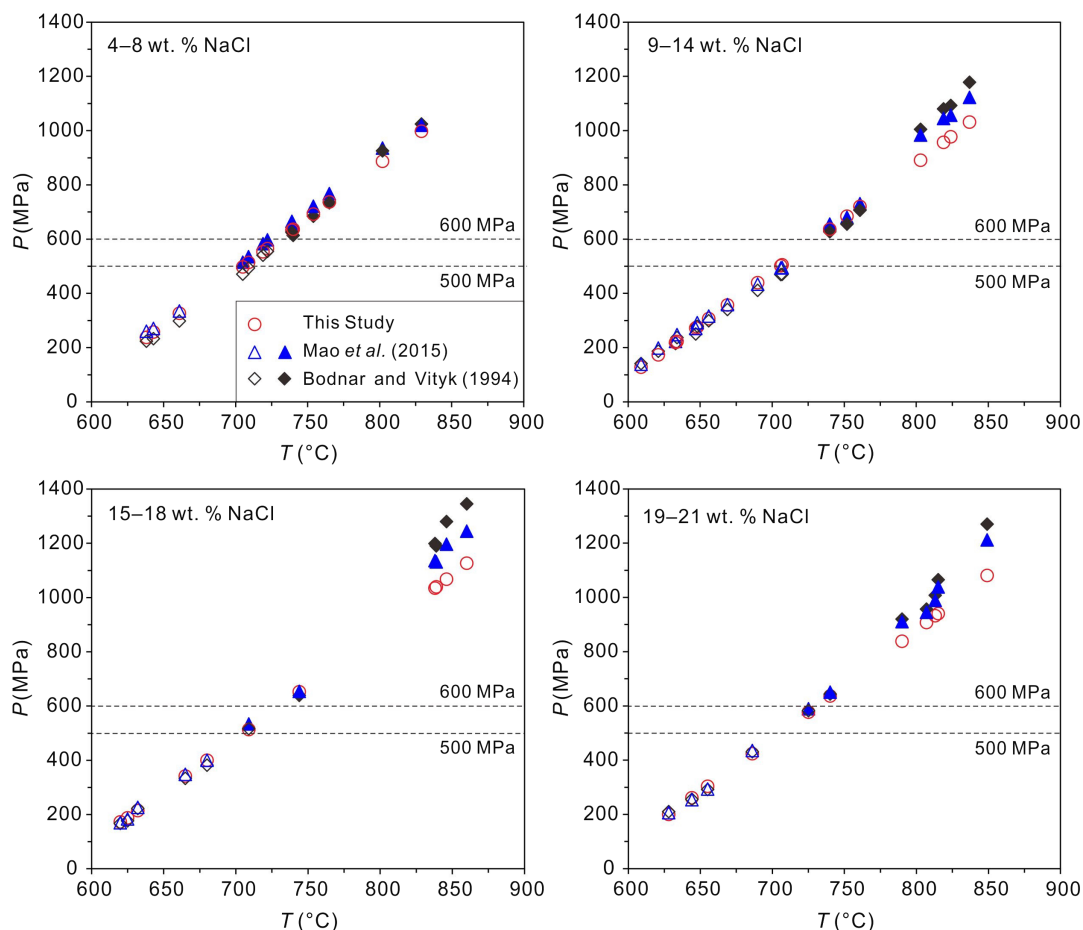
**Figure 1** Comparisons of pressures at the measured α-β quartz phase transition temperatures ($T_{tr}$s). Plotted are the α-β quartz phase transition pressures ($P_{tr}$s), which were calculated from the equation of Li and Chou (2022). Other corresponding pressures were calculated from the isochores reported by Bodnar and Vityk (1994) and Mao *et al.* (2015) and shown by the open symbols below the 600 and 500 MPa isobars, respectively; the extrapolated pressures above the two isobars are shown by the solid symbols. All data are listed in Table S-1.
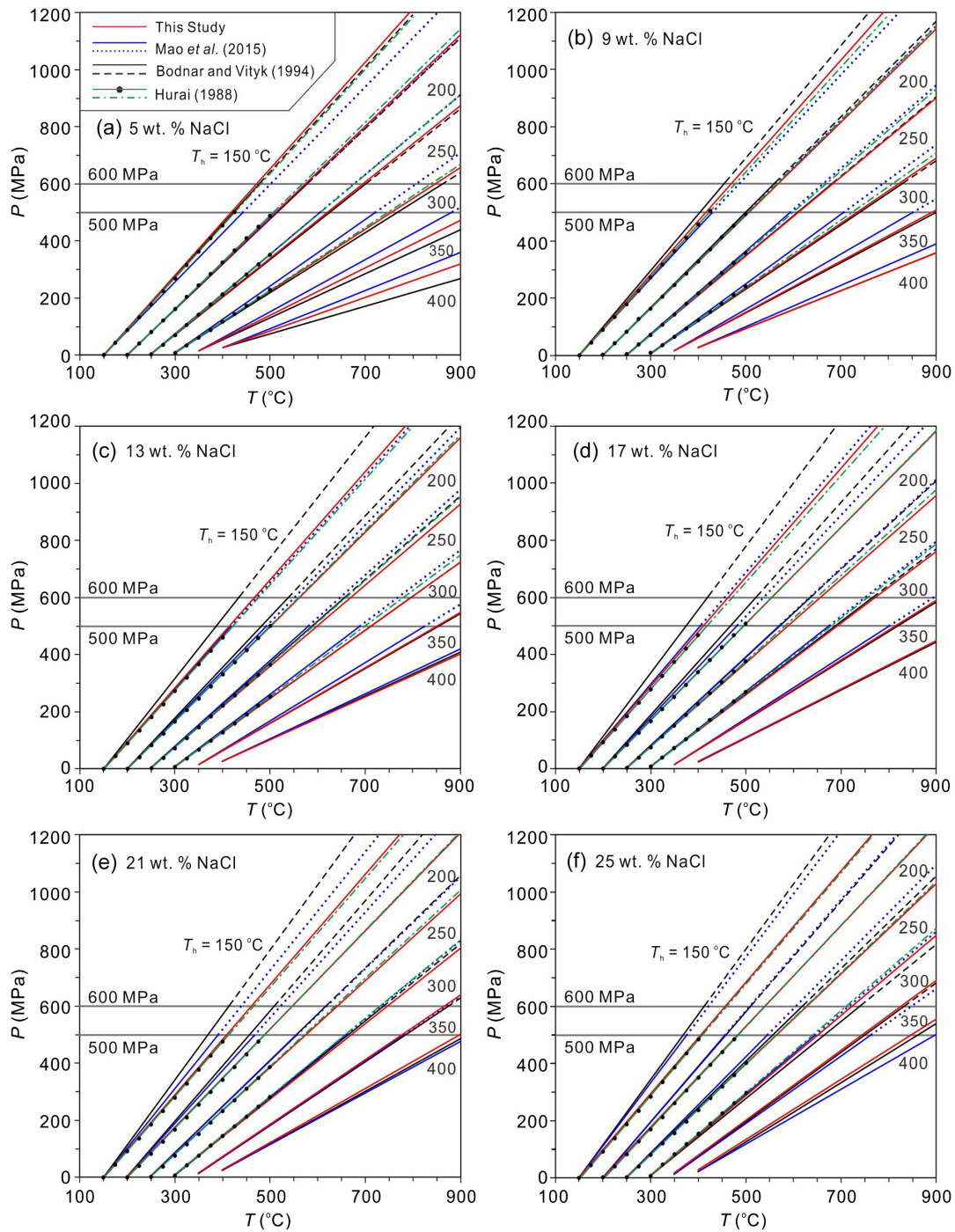
from those extrapolated from Bodnar and Vityk (1994) (Figure 2), consistent with the deviations of $P_{tr}$ values above 600 MPa shown in Figure 1.

On the other hand, the isochores of Mao *et al.* (2015) were not only fitted with the accurate EoS of $H_2O$ (IAPWS-95; Wagner and Pruß, 2002), but also calculated with the molar volume equation of the NaCl-$H_2O$ *PVTX* model from Driesner (2007) that was developed with several thousand data points available from previous literature, including those derived from SFIs. This could cause the isochore data of Mao *et al.* (2015) to be closer to ours under low $T_h$ and high salinity conditions, when compared with those of Bodnar and Vityk (1994) (Figures 1, 2c–f). Furthermore, the isochores of this study, particularly those with high salinities, agree excellently with those of Hurai (1988), which are shown in Figure 2 by the linear regression and extrapolated lines based on the data listed in Table S-2 and shown by the black dots in Figure 2. The data in Table S-2 were derived from the listed data of Hurai (1988), which summarised previously available data, especially those from Haas (1976) for vapour-saturated liquids, Hilbert (1979) for densities of solutions containing up to 25 wt. % NaCl at 20–40 MPa, 200–400 °C, and Gehrig (1980) for densities of solutions containing up to 20 wt. % NaCl at 10–300 MPa, 200–600 °C, covering 100–500 °C, ≤500 MPa and $T_h$s of 83–325 °C. The *PVT* data of Hilbert (1979) and Gehrig (1980) were collected with volume-calibrated pressure vessels under specified *P–T* conditions. Representative data of Gehrig (1980) for 20 wt. % NaCl solution are shown in

Figure S-4a as an example, to show these data were excellently presented by Hurai (1988). These features support the reliability of our isochores, implying that the isochores under our experimental conditions are approximately linear in *P–T* space and that the applicability of Equation 1 can be extended to the aqueous solutions containing 25 wt. % NaCl. Moreover, our isochores agree very well with those calculated from the density data reported by Pitzer *et al.* (1984) and Majer *et al.* (1988) within their rather limited applicable *P–T* areas (*i.e.* <100 or 40 MPa and <350 °C shown in Figure S-4b,c). However, deviations occur when extrapolating the isochores calculated from their data to higher *P–T* conditions, possibly due to the small curvature of their isochores, which are not suitable for linear extrapolations. Additionally, the *PVTX* models of Mantegazzi *et al.* (2013) and Fowler and Sherman (2020) are not considered for comparison here, as their isochores are only suitable for NaCl-$H_2O$ solutions with densities (primarily >1.0 kg/cm³) much higher than those in this study.

*Application of the isochores in the deep Earth setting.* As discussed above, our isochores of the NaCl-$H_2O$ solutions are more reliable under conditions above >600 MPa. Therefore, our isochores are expected to provide better applications in lower crustal conditions. For example, the isochores of fluid inclusions in metamorphic rocks are commonly used to determine the peak metamorphic conditions in the deep Earth setting such as a subduction zone (*e.g.*, Kawamoto *et al.*, 2018). The western Coast Mountains of British Columbia, Canada formed during terrane

**Figure 2** Comparisons of NaCl-H$_2$O isochores derived from our experimental data (red lines), those from Bodnar and Vityk (1994; black solid lines with dashed extrapolations above 600 MPa) and Mao *et al.* (2015; blue lines with dotted extrapolations above 500 MPa), and isochores (green lines with dash-dotted extrapolations above 500 MPa and 500 °C) linearly fitted with data from Hurai (1988; black circles). The homogenisation temperatures ($T_h$s) are marked.

accretion in the Jurassic and Cretaceous Periods (Wolf *et al.*, 2010). The metamorphic framework in Prince Rupert of the Coast Mountains comprises schist, gneiss, and migmatite, displaying progressive regional metamorphism. In this area, the fluid inclusions in quartz contain 25 wt. % NaCl, and the observed homogenisation $T$s (to liquid) were between 95 and 165 °C (Hurai, 1989). As shown in Figure 3, the $P$–$T$ field defined by the isochores of these fluid inclusions based on the models of Bodnar and Vityk (1994) and Mao *et al.* (2015) does not match the metamorphic $P$–$T$ path derived from associated mineral assemblages (Crawford *et al.*, 1987). However, the $P$–$T$ field

derived from our isochore model matches perfectly well with the metamorphic $P$–$T$ path.

The isochores of this study can also be used to infer the formation $P$–$T$ conditions of melt inclusions (MIs) in plutonic rocks. A fluid subsystem inside MIs usually belongs to the NaCl-H$_2$O system, existing as a shrinkage bubble. Its isochores are commonly used to estimate the MI entrapment pressure (Hurai *et al.*, 2015). By this method, the overestimation of the pressure values could be avoided, if our NaCl-H$_2$O isochores rather than those extrapolated from Bodnar and Vityk (1994) and Mao *et al.* (2015) were used.
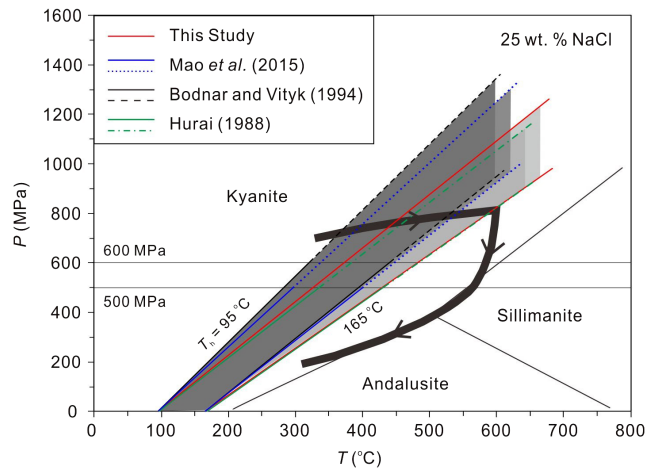
**Figure 3** Application of NaCl-H$_2$O isochores obtained in this study for the determination of the peak metamorphic conditions in Prince Rupert of the Coast Mountain, British Columbia, Canada. Hurai (1989) reported that the fluid inclusions (FIs) in quartz in this metamorphic belt have salinities of ~25 wt. % NaCl with $T_h$s (to L) of 95–165 °C. The $P$–$T$ fields (four shaded areas) defined by the FI isochores from Hurai (1988), Mao *et al.* (2015) and Bodnar and Vityk (1994), and this study are compared with the metamorphic $P$–$T$ path (thick line with arrows) derived from associated mineral assemblages (Crawford *et al.*, 1987). The lines and symbols are the same as those in Figure 2.

## References

Bassett, W.A., Shen, A.H., Bucknum, M., Chou, I-M. (1993) A new diamond anvil cell for hydrothermal studies to 2.5 GPa and from –190 to 1200 °C. *Review of scientific instruments* 64, 2340–2345. https://doi.org/10.1063/1.1143931

Bodnar, R.J. (1983) A method of calculating fluid inclusion volumes based on vapor bubble diameters and *P-V-T-X* properties of inclusion fluids. *Economic Geology* 78, 535–542. https://doi.org/10.2113/gsecongeo.78.3.535

Bodnar, R.J. (1995) Experimental determination of the *PVTX* properties of aqueous solutions at elevated temperatures and pressures using synthetic fluid inclusions: H$_2$O-NaCl as an example. *Pure and Applied Chemistry* 67, 873–880. https://doi.org/10.1351/pac199567060873

Bodnar, R.J., Sterner, S.M. (1987) Synthetic fluid inclusions. In: Ulmer, G.C., Barnes, H.L. (Eds.) *Hydrothermal Experimental Techniques*, Wiley-Interscience, New York. 423–457.

Bodnar, R.J., Vityk, M.O. (1994) Interpretation of Microthermometric data for H$_2$O-NaCl fluid inclusions. In: Vivo, B.D., Frezzoti, M.L. (Eds.) *Fluid Inclusions in Minerals: Methods and Applications*. Virginia Tech., Blacksburg, VA. 117–130.

Brown, P.E. (1989) Flincor: A microcomputer program for the reduction and investigation of fluid-inclusion data. *American Mineralogist* 74, 1390–1393.

Crawford M.L., Hollister L.S., Woodsworth G.J. (1987) Crustal deformation and regional metamorphism across a terrane boundary, Coast Plutonic Complex, British Columbia. *Tectonics* 6, 343–361. https://doi.org/10.1029/TC006i003p00343

Driesner, T. (2007) The system H$_2$O–NaCl. Part II: Correlations for molar volume, enthalpy, and isobaric heat capacity from 0 to 1000 °C, 1 to 5000 bars, and 0 to 1 $X_{NaCl}$. *Geochimica et Cosmochimica Acta* 71, 4902–4919. https://doi.org/10.1016/j.gca.2007.05.026

Fowler, S.J., Sherman, D.M. (2020) The nature of NaCl–H$_2$O deep fluids from *ab initio* molecular dynamics at 0.5–4.5 GPa, 20–800 °C, and 1–14 m NaCl. *Geochimica et Cosmochimica Acta* 277, 243–264. https://doi.org/10.1016/j.gca.2020.03.031

Gerhig, M. (1980) Phasengleichgewichte und PVT-Daten temiirer Mischungen aus Wasser, Kohlendioxid und Natriumchlorid bis 3 kbar und 550°C. Ph.D. dissertation, Universitat Karlsruhe, 109p.

Haas, J.L. (1976) Physical properties of the coexisting phases and thermochemical properties of the H$_2$O component in boiling NaCl solutions. *United States Geology Survey Bulletin* 1421-A. https://pubs.usgs.gov/bul/1421a/report.pdf

Haar, L., Gallagher, J.S., Kell, G.S. (1984) *NBS/NRC steam tables: thermodynamic and transport properties and computer programs for vapor and liquid states of water in SI units*. Hemisphere Publishing Corp, Washington, D.C.

Hilbert, R. (1979) PVT-Daten von Wasser und von wässrigen Natriumchlorid-Lösungen. PhD thesis, Universität Karlsruhe, 212p.

Hurai, V. (1988) *P–V–T–X* tables of water and 1–25 weight percent NaCl-H$_2$O solutions to 500 °C and 500 × 10$^5$ Pa. *Acta Geologica et Geographica Universitatis Comenianae* 44, 101–135.

Hurai, V. (1989) Basic program for interpretation of microthermometric data from H$_2$O and H$_2$O-NaCl fluid inclusions. *Computational Geosciences* 15, 135–142. https://doi.org/10.1016/0098-3004(89)90060-5

Hurai, V., Huraiova M., Slobodnik M., Thomas R. (2015) *Geofluids—Developments in Microthermometry, Spectroscopy, Thermodynamics, and Stable Isotopes*. Elsevier, Amsterdam, The Netherlands, 489p. https://doi.org/10.1016/C2014-0-03099-7

Kawamoto, T., Hertwig, A., Schertl, H.-P., Maresch, W.V. (2018) Fluid inclusions in jadeitite and jadeite-rich rock from serpentinite mélanges in northern

## Conclusions

The isochores of NaCl-H$_2$O solutions with salinities of up to 21 wt. % NaCl (applicable up to 25 wt. % NaCl), measured in the HDAC experiments by using the re-fitted α-β quartz $P$–$T$ boundary of Li and Chou (2022), were extended to ~900 °C and ~1.2 GPa.

At pressures above 600 MPa, our isochores are considered to be reliable and accurate relative to previous ones and their extrapolations, particularly those derived from analyses of SFIs. Therefore, our isochores are more suitable to be applied for the interpretations of geological processes involving NaCl-H$_2$O fluids in the lower crust.

Our experiments also suggest a fast method for the accurate measurement of isochores of geologically important saline solutions with solutes of LiCl, NaCl, KCl, CaCl$_2$, *etc.*, and their mixtures by using HDAC and the newly calibrated α-β quartz $P$–$T$ boundary of Li and Chou (2022) under wide $P$–$T$ conditions.

## Ackowledgements

## Additional Information

**Supplementary Information** accompanies this letter at https://www.geochemicalperspectivesletters.org/article2429.

Hispaniola: Trapped ambient fluids in a cold subduction channel. *Lithos* 308–309, 227–241. https://doi.org/10.1016/j.lithos.2018.02.024

Li, J.K., Chou, I. M., Bassett, W.A., Wang, X. (2020) A new type of hydrothermal diamond-anvil cell with cooling system. *Review of Scientific Instruments* 91, 053104. https://doi.org/10.1063/1.5143596

Li, S.H., Chou, I-M. (2022) Refinement of the α-β quartz phase boundary based on in situ Raman spectroscopy measurements in hydrothermal diamond-anvil cell and an evaluated equation of state of pure $H_2O$. *Journal of Raman Spectroscopy* 53, 1471–1482. https://doi.org/10.1002/jrs.6367

Mantegazzi, D., Sanchez-Valle, C., Driesner, T. (2013) Thermodynamic properties of aqueous NaCl solutions to 1073 K and 4.5 GPa, and implications for dehydration reactions in subducting slabs. *Geochimica et Cosmochimica Acta* 121, 263–290. https://doi.org/10.1016/j.gca.2013.07.015

Majer, V., Gates, J.A., Inglese, A., Wood, R.H. (1988) Volumetric properties of aqueous NaCl solutions from 0.0025 to 5.0 mol kg1, 323 to 600 K, and 0.1 to 40 MPa. *The Journal of Chemical Thermodynamics* 20, 949–968. https://doi.org/10.1016/0021-9614(88)90224-8

Mao, S., Hu, J., Zhang, Y., Meng, X.L. (2015) A predictive model for the PVTX properties of $CO_2$–$H_2O$–NaCl fluid mixture up to high temperature and high pressure. *Applied Geochemistry* 54, 54–64. https://doi.org/10.1016/j.apgeochem.2015.01.003

Pitzer, K.S., Peiper, J.C., Busey, R.H. (1984) Thermodynamic properties of aqueous sodium chloride solutions. *Journal of Physical and Chemical Reference Data* 13, 1–102. https://doi.org/10.1063/1.555709

Schmidt, C., Ziemann, M.A. (2000) In-situ Raman spectroscopy of quartz: A pressure sensor for hydrothermal diamond-anvil cell experiments at elevated temperatures. *American Mineralogist* 85, 1725–1734. https://doi.org/10.2138/am-2000-11-1216

Shen, A.H., Bassett, W.A., Chou, I-M. (1993) The alpha-beta quartz transition at high temperatures and pressures in a diamond-anvil cell by laser interferometry. *American Mineralogist* 78, 694–698.

Sullivan N.A., Zoltán Z., Brenan J.M., Hinde J.C., Yin Y.W. (2022) The solubility of gold and palladium in magmatic brines: Implications for PGE enrichment in mafic-ultramafic and porphyry environments. *Geochimica et Cosmochimica Acta* 316, 230–252. https://doi.org/10.1016/j.gca.2021.09.010

Wagner, W., Pruβ, A. (2002) The IAPWS formulation 1995 for the thermodynamic properties of ordinary water substance for general and scientific use. *Journal of Physical and Chemical Reference Data* 31, 387–535. https://doi.org/10.1063/1.1461829

Wolf, D.E., Andronicos, C.L., Vervoort, J.D., Mansfield, M.R., Chardon, D. (2010) Application of Lu–Hf garnet dating to unravel the relationships between deformation, metamorphism and plutonism: An example from the Prince Rupert area, British Columbia. *Tectonophysics* 485, 62–77. https://doi.org/10.1016/j.tecto.2009.11.020

Zhang, Y.G., Frantz, J.D. (1987) Determination of the homogenization temperatures and densities of supercritical fluids in the system NaCl-KCl-$CaCl_2$-$H_2O$ using synthetic fluid inclusions. *Chemical Geology* 64, 335–350. https://doi.org/10.1016/0009-2541(87)90012-X

# *In situ* determination of NaCl-H₂O isochores up to 900 °C and 1.2 GPa in a hydrothermal diamond anvil-cell

**J.K. Li, I-M. Chou, X. Wang**

## Supplementary Information

The Supplementary Information includes:

- ➢ Experimental methods
- ➢ Tables S-1 and S-2
- ➢ Figures S-1 to S-4
- ➢ Supplementary Information References

## Experimental methods

Isochores of the $H_2O$-NaCl system were measured, as illustrated in Figure S-1, by using a Bassett VT-type hydrothermal diamond-anvil cell (HDAC; Li *et al.* 2016), with a newly designed cooling system (Li *et al.* 2020), and a Raman spectrometer. The HDAC sample chamber is a hole (0.5 mm diameter) at the center of the annular rhenium gasket (3 mm diameter and 0.125 mm thick), compressed and sealed by the two parallel diamond anvils (Figure S-2a; Bassett *et al.*, 1993). The sample chamber was heated externally by using two tungsten carbide furnaces, each of which was wrapped with a heating resistance wire. The heating power to the heaters was controlled through a temperature controller (PES1300; Li *et al.* 2020). During cooling, the sample chamber was cooled by a stream of nitrogen, which was cooled through a stainless steel coil immersed in a liquid nitrogen Dewar, as described in Li *et al.* (2020). The temperatures were measured using two K-type thermocouples from Omega Engineering with their tips attached separately to the two diamond anvils. The new thermocouples were calibrated by measuring the triple point of $H_2O$ (0.01 °C), the eutectic point of NaCl solution (-21.2 °C), and the melting points of $NaNO_3$ (306.8 °C) and NaCl (800.5 °C) before experiments, and they were checked again after each experiment to confirm their reliabilities. The reported temperatures are accurate to ± 0.5 °C. A JY/Horiba LabRAM HR Evolution Raman system was used, with an SLWD 20× Olympus objective (0.4 numerical aperture), a 532 nm laser excitation, a grating of 1800-grooves/mm, spectral resolution of 0.2 cm$^{-1}$, and ~40 mW laser light focused on the sample during the measurement.

At the beginning of each set of isochore experiments, a quartz chip (80 μm thick; as a pressure sensor) from the Jiajika pegmatites, Sichuan, China (Li and Chou, 2016) and $H_2O$-NaCl solution were loaded and sealed in the sample chamber with a vapour bubble (Figure S-2b). The solutions were prepared with salinities of 2, 5, 10, and 13 wt. % NaCl. Subsequently, considering the new rhenium gasket could be deformed during heating, we heated the sample chamber from ambient to 850 ºC in several cycles until the difference of the two vapor-disappearing (*i.e.*, vapour to liquid homogenization) temperatures ($T_h$s), in the two adjacent cycles was less than 1 °C to ensure that the sample chamber did have a negligible volume change in the following heating cycle. Such a Re gasket training procedure is the same as that described by Li and Chou (2022).

In the following heating cycle after the Re gasket was trained, we collected the in-situ Raman spectra of quartz in the HDAC sample chamber while the temperature increased from ambient to the temperature above the α-β quartz phase transition temperature ($T_{tr}$), and the heating rate was reduced from 5 °C/min to 1 °C/min while the temperature was close to $T_{tr}$. The $T_{tr}$ was determined by the abrupt ~128-$cm^{-1}$ Raman shift of α-quartz as shown in Figure S-1b. At each temperature, the Raman spectrum of quartz, collected for 20–60 s with two accumulations, was repeatedly collected for 3–5 times until the Raman shifts of the 128-$cm^{-1}$ band were constant. Details of this Raman spectroscopic criterion were described by Li and Chou (2022). After a heating cycle, we cooled the sample chamber to the ambient temperature and then repeated the Raman spectra collection procedures during the following heating cycle to check the observed $T_{tr}$. In the two consecutive heating cycles, we also compared the $T_h$s to further ensure that the volume of the sample chamber is kept constant. Subsequently, we tightened the driver screws of HDAC to reduce the volume of the sample chamber and thus increase the bulk $H_2O$-NaCl solution density and then repeated the above experimental procedures to obtain the $T_{tr}$ under a higher pressure condition.

Finally, after the sample chamber was cooled, the final melting temperature of ice ($T_{ice}$) in the $H_2O$-NaCl system was measured and the salinity of the fluid in the sample chamber was calculated according to the equation of Bodnar (1993).

# Supplementary Tables

**Table S-1** Experimental results for the measurements of the isochores of NaCl-H$_2$O solutions loaded in the sample chamber of a hydrothermal diamond-anvil cell

| [a]No. | [b]$T_{ice}$ (°C) | [c]$Sal$ (wt. % NaCl) | [d]$T_h$ (°C) | [e]$P_h$ (MPa) | [f]$T_{tr}$ (°C) | [g]$P_{tr}$ (MPa) | [h]$P_{trB}$ (MPa) | [i]$P_{trM}$ (MPa) | [j]$P_{trC}$ (MPa) | [k]$P_{error}$ (%) | [l]$Slp_{error}$ (%) |
|---|---|---|---|---|---|---|---|---|---|---|---|
| 1 | −3.5 | 5.7 | 359.7 | 17.85 | 638 | 238.11 | 223.81 | 260.76 | 238.91 | 0.34 | 0.36 |
| 2 | −3.5 | 5.7 | 357.1 | 17.32 | 643 | 257.26 | 232.94 | 270.61 | 248.08 | 3.57 | 3.83 |
| 3 | −4.1 | 6.6 | 338.0 | 13.67 | 661 | 326.54 | 298.23 | 334.94 | 309.30 | 5.28 | 5.51 |
| 4 | −3.6 | 5.9 | 290.0 | 7.17 | 705 | 498.07 | 471.35 | 515.12 | 481.70 | 3.29 | 3.33 |
| 5 | −3.7 | 6.0 | 274.4 | 5.66 | 719 | 553.30 | 540.89 | 583.61 | 549.80 | 0.63 | 0.64 |
| 6 | −3.7 | 6.0 | 271.4 | 5.40 | 722 | 565.17 | 555.04 | 597.43 | 563.72 | 0.26 | 0.26 |
| 7 | −3.7 | 6.0 | 258.0 | 4.35 | 739 | 632.74 | 625.34 | 665.57 | 633.06 | 0.05 | 0.05 |
| 8 | −3.7 | 6.0 | 247.9 | 3.67 | 754 | 692.74 | 684.25 | 721.70 | 691.26 | 0.21 | 0.21 |
| 9 | −3.7 | 6.0 | 239.4 | 3.17 | 765 | 736.96 | 733.72 | 767.66 | 740.12 | 0.43 | 0.43 |
| 10 | −4.3 | 6.9 | 210.2 | 1.82 | 802 | 887.15 | 925.70 | 935.80 | 924.50 | 4.21 | 4.22 |
| 11 | −4.6 | 7.3 | 200.0 | 1.47 | 829 | 998.14 | 1024.31 | 1019.97 | 1016.97 | 1.89 | 1.89 |
| 12 | −4.3 | 6.9 | 263.0 | 4.69 | 740 | 636.72 | 613.98 | 654.84 | 620.47 | 2.55 | 2.57 |
| 13 | −4.6 | 7.3 | 287.5 | 6.84 | 709 | 513.82 | 493.89 | 535.38 | 501.59 | 2.38 | 2.41 |
| 14 | −9.0 | 12.8 | 442.0 | 37.28 | 609 | 127.82 | 141.35 | 138.99 | 134.31 | 5.08 | 7.18 |
| 15 | −6.7 | 10.1 | 394.8 | 25.13 | 621 | 173.29 | 187.11 | 198.79 | 186.29 | 7.50 | 8.78 |
| 16 | −9.0 | 12.8 | 391.4 | 23.70 | 633 | 219.00 | 215.14 | 222.93 | 213.89 | 2.33 | 2.62 |
| 17 | −9.0 | 12.8 | 377.8 | 20.62 | 634 | 222.82 | 236.89 | 248.00 | 237.27 | 6.49 | 7.15 |
| 18 | −6.4 | 9.7 | 366.4 | 18.69 | 647 | 272.61 | 250.04 | 270.44 | 252.72 | 7.30 | 7.83 |
| 19 | −10.4 | 14.4 | 365.1 | 17.73 | 648 | 276.45 | 278.78 | 291.72 | 281.30 | 1.75 | 1.88 |
| 20 | −9.2 | 13.1 | 355.0 | 15.99 | 656 | 307.24 | 299.24 | 316.66 | 301.70 | 1.80 | 1.90 |
| 21 | −10.4 | 14.4 | 345.0 | 14.04 | 669 | 357.50 | 340.46 | 358.89 | 343.70 | 3.86 | 4.02 |
| 22 | −10.4 | 14.4 | 325.1 | 10.93 | 690 | 439.24 | 411.41 | 434.41 | 413.62 | 5.83 | 5.98 |
| 23 | −10.8 | 14.8 | 312.0 | 9.14 | 706 | 502.00 | 469.24 | 493.48 | 469.18 | 6.54 | 6.66 |
| 24 | −10.4 | 14.4 | 311.0 | 9.04 | 707 | 505.94 | 470.39 | 495.69 | 470.45 | 7.02 | 7.14 |
| 25 | −9.8 | 13.7 | 272.0 | 5.12 | 752 | 684.71 | 655.66 | 680.62 | 643.26 | 6.05 | 6.10 |
| 26 | −8.9 | 12.7 | 260.0 | 4.27 | 761 | 720.86 | 706.60 | 730.73 | 691.56 | 4.06 | 4.09 |
| 27 | −9.2 | 13.1 | 211.8 | 1.79 | 803 | 891.24 | 1004.69 | 983.63 | 947.77 | 6.34 | 6.35 |
| 28 | −9.2 | 13.1 | 203.2 | 1.51 | 819 | 956.90 | 1079.95 | 1044.71 | 1011.82 | 5.74 | 5.75 |
| 29 | −8.4 | 12.2 | 200.0 | 1.42 | 824 | 977.50 | 1092.46 | 1057.04 | 1030.35 | 5.41 | 5.42 |
| 30 | −8.6 | 12.4 | 272.0 | 5.18 | 740 | 636.72 | 627.20 | 655.88 | 619.28 | 2.74 | 2.76 |
| 31 | −7.7 | 11.3 | 186.8 | 1.08 | 837 | 1031.24 | 1178.32 | 1122.40 | 1111.04 | 7.74 | 7.75 |
| 32 | −12.0 | 16.0 | 432.7 | 33.28 | 620 | 173.29 | 167.83 | 169.95 | 164.86 | 4.86 | 6.02 |
| 33 | −12.5 | 16.4 | 428.0 | 31.83 | 625 | 188.50 | 177.11 | 184.26 | 176.14 | 6.56 | 7.89 |
| 34 | −11.7 | 15.7 | 394.0 | 23.65 | 632 | 215.18 | 222.62 | 227.04 | 224.11 | 4.15 | 4.66 |
| 35 | −11.7 | 15.7 | 349.6 | 14.66 | 665 | 342.00 | 333.62 | 348.90 | 337.54 | 1.30 | 1.36 |

| No. | $T_{ice}$ | Sal | $T_h$ | $P_h$ | $T_{tr}$ | $P_{tr}$ | $P_{trB}$ | $P_{trM}$ | $P_{trC}$ | $P_{error}$ | $Slp_{error}$ |
|---|---|---|---|---|---|---|---|---|---|---|---|
| 36 | −11.7 | 15.7 | 335.5 | 12.34 | 680 | 400.23 | 382.20 | 400.67 | 385.40 | 3.70 | 3.82 |
| 37 | −13.8 | 17.6 | 304.6 | 8.02 | 709 | 513.82 | 517.00 | 534.26 | 512.37 | 0.28 | 0.29 |
| 38 | −14.1 | 17.9 | 283.3 | 5.85 | 744 | 652.70 | 639.34 | 654.28 | 623.08 | 4.54 | 4.58 |
| 39 | −11.9 | 15.9 | 196.0 | 1.26 | 838 | 1035.39 | 1199.83 | 1136.90 | 1090.06 | 5.28 | 5.29 |
| 40 | −12.5 | 16.4 | 187.0 | 1.04 | 846 | 1068.61 | 1280.51 | 1196.92 | 1148.28 | 7.46 | 7.46 |
| 41 | −12.5 | 16.4 | 199.0 | 1.34 | 839 | 1039.54 | 1191.24 | 1132.31 | 1081.03 | 3.99 | 4.00 |
| 42 | −11.9 | 15.9 | 180.0 | 0.89 | 860 | 1127.00 | 1345.65 | 1245.30 | 1203.58 | 6.80 | 6.80 |
| 43 | −16.6 | 19.9 | 413.0 | 26.84 | 628 | 199.92 | 210.48 | 206.56 | 217.03 | 8.56 | 9.88 |
| 44 | −17.0 | 20.2 | 393.0 | 22.25 | 644 | 261.10 | 255.66 | 254.24 | 263.68 | 0.99 | 1.08 |
| 45 | −17.0 | 20.2 | 378.0 | 19.15 | 655 | 303.39 | 292.20 | 293.38 | 300.45 | 0.97 | 1.03 |
| 46 | −18.3 | 21.2 | 334.0 | 11.43 | 686 | 423.62 | 430.64 | 435.95 | 434.01 | 2.45 | 2.52 |
| 47 | −18.3 | 21.2 | 300.0 | 7.22 | 725 | 577.06 | 582.20 | 589.64 | 572.05 | 0.87 | 0.88 |
| 48 | −18.0 | 21.0 | 288.0 | 6.08 | 740 | 636.72 | 643.44 | 650.73 | 625.94 | 1.69 | 1.71 |
| 49 | −17.4 | 20.5 | 240.4 | 2.84 | 790 | 838.20 | 920.29 | 910.66 | 856.45 | 2.18 | 2.18 |
| 50 | −17.4 | 20.5 | 220.8 | 1.98 | 815 | 940.44 | 1065.59 | 1038.90 | 972.15 | 3.37 | 3.38 |
| 51 | −17.4 | 20.5 | 196.8 | 1.23 | 849 | 1081.10 | 1270.38 | 1211.77 | 1130.43 | 4.56 | 4.57 |
| 52 | −16.2 | 19.6 | 229.2 | 2.34 | 813 | 932.23 | 1007.95 | 988.78 | 929.32 | 0.31 | 0.31 |
| 53 | −16.2 | 19.6 | 237.0 | 2.70 | 807 | 907.62 | 957.09 | 944.96 | 889.38 | 2.01 | 2.02 |
| Average value | | | | | | | | | | 3.69 | 3.90 |

Note:

[a]No.: experimental number;

[b]$T_{ice}$: ice point of NaCl-$H_2O$ solution measured in HDAC with the cooling system after the Raman spectroscopic measurements of the α-β quartz phase transition;

[c]$Sal$: salinity of NaCl-$H_2O$ solution calculated from Bodnar (1993);

[d]$T_h$: vapor bubble-disappearing temperature in the HDAC sample chamber;

[e]$P_h$: pressure at $T_h$ calculated with the equation of Bodnar (1983);

[f]$T_{tr}$: the measured α-β quartz phase transition temperature;

[g]$P_{tr}$: the sample pressure at $T_{tr}$ calculated according to the refined α-β quartz $P$–$T$ boundary of Li and Chou (2022);

[h]$P_{trB}$: the sample pressure at $T_{tr}$ calculated from the NaCl-$H_2O$ isochore of Bodnar and Vityk (1994);

[i]$P_{trM}$: the sample pressure at $T_{tr}$ calculated from the NaCl-$H_2O$ isochore of Mao $et~al.$ (2015);

[j]$P_{trC}$: the sample pressure at $T_{tr}$ calculated from the fitted Equations (1) shown in the text;

[k]$P_{error}$: the error between [g]$P_{tr}$ and [j]$P_{trC}$. [k]$P_{error} = |^{g}P_{tr} - {}^{j}P_{trC}| / {}^{g}P_{tr} \times 100\%$.

[i]$Slp_{error}$: the slope errors between measured isochores (Isochore$_{MS}$) and fitted isochores (Isochore$_{FS}$), which were determined with $[(T_h, P_h), (T_{tr}, P_{tr})]$ and $[(T_h, P_h), (T_{tr}, P_{tr}c)]$, respectively. [i]$Slp_{error} = |$Isochore$_M -$ Isochore$_F|/$ Isochore$_M \times 100\%$.

**Table S-2** Pressures at specified temperatures along the isochores of NaCl-H$_2$O solutions interpolated from the listed values of Hurai (1988)

| [a]$T_h$ (°C) | [b]Temperature (°C) on the isochore | | | | | | | | | | | | | | |
|---|---|---|---|---|---|---|---|---|---|---|---|---|---|---|---|
| | 150 °C | 175 | 200 | 225 | 250 | 275 | 300 | 325 | 350 | 375 | 400 | 425 | 450 | 475 | 500 |
| | [c]Pressure (MPa) on the isochore | | | | | | | | | | | | | | |
| **5 wt. % NaCl** | | | | | | | | | | | | | | | |
| 150 | [c]40 ([d]−3.4) | 437 (−1.0) | 87.7 (0.7) | 132.4 (1.7) | 177.8 (1.9) | 223.6 (1.8) | 270.0 (1.1) | 316.3 (0.4) | 362.7 (−0.3) | 408.8 (−0.7) | 454.7 (−0.9) | 500.7 (−1.3) | [e]\ | \ | \ |
| 200 | | | 1.5 (−1.3) | 41.5 (−0.4) | 81.4 (0.4) | 122.0 (0.5) | 162.8 (0.6) | 204.0 (0.1) | 244.0 (0.9) | 284.8 (0.8) | 326.0 (0.4) | 367.9 (−0.7) | 408.7 (−0.8) | 449.2 (−0.6) | 489.1 (0.3) |
| 250 | | | | | 3.9 (−1.6) | 37.5 (−0.2) | 710 (1.2) | 105.7 (1.5) | 141.4 (0.7) | 177.1 (0.0) | 212.6 (−0.6) | 247.7 (−0.7) | 282.7 (−0.7) | 317.2 (−0.3) | 351.0 (0.8) |
| 300 | | | | | | | 8.3 (−1.7) | 34.1 (0.1) | 61.4 (0.4) | 88.9 (0.4) | 116.6 (0.3) | 144.3 (0.2) | 172.4 (−0.3) | 200.3 (−0.6) | 228.2 (−0.9) |
| **9 wt. % NaCl** | | | | | | | | | | | | | | | |
| 150 | −25 | 44.3 (−0.9) | 89.0 (0.4) | 133.9 (1.3) | 179.5 (1.7) | 226.3 (0.8) | 271.6 (1.4) | 317.9 (1.0) | 364.5 (0.3) | 411.0 (−0.3) | 457.6 (−1.0) | 504.3 (−1.8) | \ | \ | \ |
| 200 | | | 1.5 (−0.9) | 41.8 (−0.1) | 83.0 (−0.3) | 126.4 (−2.5) | 163.9 (1.0) | 205.1 (0.9) | 244.9 (2.2) | 286.2 (2.0) | 328.0 (1.2) | 370.8 (−0.5) | 412.3 (−0.9) | 453.8 (−1.4) | 494.2 (−0.7) |
| 250 | | | | | 3.7 (−2.1) | 37.5 (−0.1) | 71.4 (1.7) | 107.0 (1.8) | 143.8 (0.7) | 180.3 (−0.1) | 216.8 (−0.9) | 2527. (−1.1) | 288.4 (−1.1) | 323.1 (−0.1) | 357.5 (1.2) |
| 300 | | | | | | | 8.1 (−2.0) | 34.9 (0.5) | 63.9 (0.7) | 93.0 (0.9) | 122.5 (0.6) | 151.8 (0.5) | 181.7 (−0.2) | 211.2 (−0.4) | 240.8 (−0.8) |
| **13 wt. % NaCl** | | | | | | | | | | | | | | | |
| 150 | 4 (−27) | 44.8 (−0.8) | 90.0 (0.2) | 135.3 (1.2) | 181.2 (1.5) | 227.1 (1.8) | 274.0 (1.2) | 320.6 (0.8) | 367.7 (−0.1) | 414.9 (−1.0) | 462.1 (−2.0) | \ | \ | \ | \ |
| 200 | | | 1.4 (−2.4) | 41.9 (−1.2) | 82.5 (0.0) | 123.8 (0.4) | 165.2 (0.8) | 206.6 (1.1) | 247.1 (2.3) | 289.2 (2.0) | 331.5 (1.4) | 375.1 (−0.5) | 417.3 (−1.0) | 459.8 (−1.7) | 501.1 (−1.3) |
| 250 | | | | | 3.6 (−2.3) | 37.9 (−0.1) | 72.5 (1.9) | 109.1 (1.8) | 146.7 (0.8) | 184.1 (0.0) | 221.5 (−0.9) | 258.3 (−1.1) | 295.0 (−1.2) | 330.4 (−0.1) | 365.8 (1.1) |
| 300 | | | | | | | 7.8 (−1.7) | 36.6 (0.4) | 67.3 (0.6) | 98.1 (0.7) | 129.2 (0.5) | 160.2 (0.4) | 191.7 (−0.2) | 222.7 (−0.3) | 254.0 (−0.7) |
| **17 wt. % NaCl** | | | | | | | | | | | | | | | |
| 150 | 4 | 45.2 | 90.9 | 136.7 | 183.1 | 229.5 | 276.9 | 324.5 | 372.4 | 420.3 | 468.2 | \ | \ | \ | \ |

| $T_h$ | 1 | 2 | 3 | 4 | 5 | 6 | 7 | 8 | 9 | 10 | 11 | 12 | 13 | 14 | 15 |
|---|---|---|---|---|---|---|---|---|---|---|---|---|---|---|---|
|  | (−30) | (−0.9) | (0.2) | (1.2) | (1.7) | (2.2) | (1.6) | (0.9) | (−0.2) | (−1.2) | (−2.3) |  |  |  |  |
| 200 | 1.4 (−3.1) | 41.9 (−1.3) | 82.8 (0.3) | 124.7 (0.7) | 166.6 (1.3) | 207.8 (2.5) | 250.7 (2.0) | 293.4 (1.7) | 336.7 (0.8) | 380.8 (−0.9) | 423.8 (−1.5) | 467.2 (−2.6) | 506.7 (0.3) |  |  |
| 250 |  |  | 3.6 (−2.3) | 37.9 (−0.1) | 72.5 (1.9) | 109.1 (1.8) | 146.7 (0.8) | 184.1 (0.0) | 221.5 (−0.9) | 258.3 (−1.1) | 295.0 (−1.2) | 330.4 (−0.1) | 365.8 (1.1) |  |  |
| 300 |  |  | 7.5 (−0.8) | 39.2 (0.2) | 71.5 (0.4) | 104.2 (0.2) | 136.8 (0.2) | 169.4 (0.2) | 202.3 (−0.1) | 234.9 (−0.2) | 267.6 (−0.3) |  |  |  |  |
| **21 wt. % NaCl** |  |  |  |  |  |  |  |  |  |  |  |  |  |  |  |
| 150 | 4 (−39) | 45.3 (−1.1) | 91.5 (0.4) | 138.0 (1.6) | 185.2 (2.0) | 232.2 (2.7) | 280.5 (2.1) | 329.4 (0.9) | 378.3 (−0.4) | 427.3 (−1.7) | 475.9 (−2.6) | \ | \ | \ | \ |
| 200 | 1.3 (−4.4) | 41.6 (−1.3) | 82.9 (0.8) | 125.7 (1.3) | 168.1 (2.2) | 210.4 (3.3) | 255.6 (1.4) | 299.2 (1.1) | 343.5 (0.2) | 387.8 (−0.8) | 431.7 (−1.4) | 476.0 (−2.4) | \ |  |  |
| 250 |  |  | 3.3 (−2.6) | 39.7 (−0.3) | 77.2 (0.8) | 115.8 (0.8) | 153.5 (1.8) | 192.7 (1.3) | 232.0 (0.5) | 271.3 (−0.1) | 310.5 (−0.7) | 349.2 (−0.7) | 3878 (−0.7) |  |  |
| 300 |  |  | 72. (0.8) | 42.7 (−0.4) | 76.6 (−0.1) | 111.3 (−0.5) | 145.3 (−0.2) | 179.4 (0.0) | 213.6 (0.0) | 247.8 (0.1) | 281.8 (0.3) |  |  |  |  |
| **25 wt. % NaCl** |  |  |  |  |  |  |  |  |  |  |  |  |  |  |  |
| 150 | 4 (−51) | 45.3 (−1.3) | 91.9 (0.7) | 139.2 (2.2) | 187.4 (2.7) | 235.4 (3.4) | 284.9 (2.6) | 335.3 (0.9) | 385.6 (−0.7) | 435.9 (−2.3) | 485.2 (−2.9) | \ | \ | \ |  |
| 200 | 1.2 (−5.9) | 41.1 (−1.3) | 82.8 (1.4) | 126.6 (2.1) | 169.7 (3.4) | 212.7 (4.9) | 261.8 (0.2) | 306.5 (0.0) | 351.9 (−1.0) | 396.2 (−0.8) | 441.1 (−1.2) | 486.2 (−1.9) | \ |  |  |
| 250 |  |  | 3.2 (−2.5) | 41.1 (−0.6) | 80.8 (−0.4) | 120.4 (−0.1) | 157.6 (2.5) | 197.5 (24) | 238.0 (1.8) | 278.8 (0.8) | 319.5 (0.0) | 360.7 (−1.3) | 401.5 (−2.3) |  |  |
| 300 |  |  | 6.9 (3.0) | 47.0 (−1.1) | 82.6 (−0.7) | 119.5 (−1.6) | 154.6 (−0.8) | 190.2 (−0.4) | 225.6 (0.2) | 261.3 (0.4) | 2966 (1.1) |  |  |  |  |

[a] $T_h$, liquid-vapor homogenization (to liquid phase) temperature.

[b] specified temperature on the isochore of NaCl-$H_2O$ solution.

[c] pressure, interpolated from the listed values in Hurai (1988), at the specified temperature on the isochore corresponding to the $T_h$.

[d] deviation of the pressure, calculated with the linear equation that fitted the $P$–$T$ data of the isochore corresponding to the $T_h$, from the [c] pressure.

[e] not available; the data of Hurai (1988) are below ~500 MPa.

## Supplementary Figures
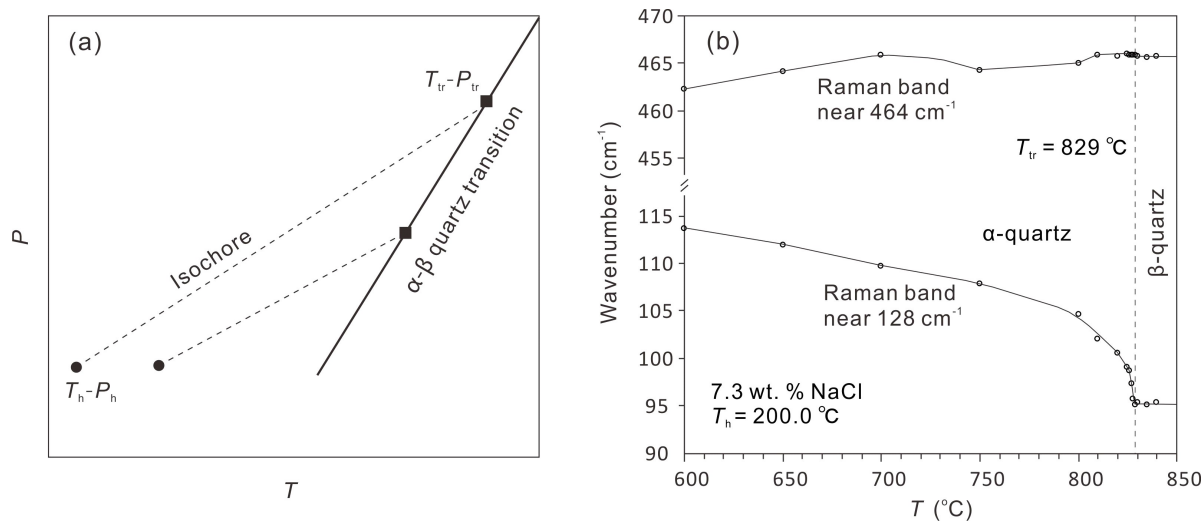


**Figure S-1 (a)** Diagram showing the isochores (dashed lines) of the fluid inside the HDAC sample chamber determined by α-β quartz transition temperature ($T_{tr}$) –pressure ($P_{tr}$) boundary (squares on the solid α-β quartz phase transition line) and the L–V homogenization temperature (to L; $T_h$) –pressure ($P_h$) (dots). **(b)** Diagram illustrating the advantage of using the Raman shift of the quartz band near 128 cm$^{-1}$ relative to 464 cm$^{-1}$ for the determination of the $T_{tr}$, during heating, for an NaCl-H$_2$O solution (with salinity of 7.3 wt. % NaCl and $T_h$ of 200 °C) loaded in the HDAC sample chamber; plotted are the data from Exp. 11 listed in Table S-1, and $T_{tr}$ at 829 °C is marked by the vertical dashed line. The two solid lines show the trends of the temperature dependence of the Raman shifts for the 128 (lower) and 464-cm$^{-1}$ (upper) quartz bands in both α- and β-quartz.
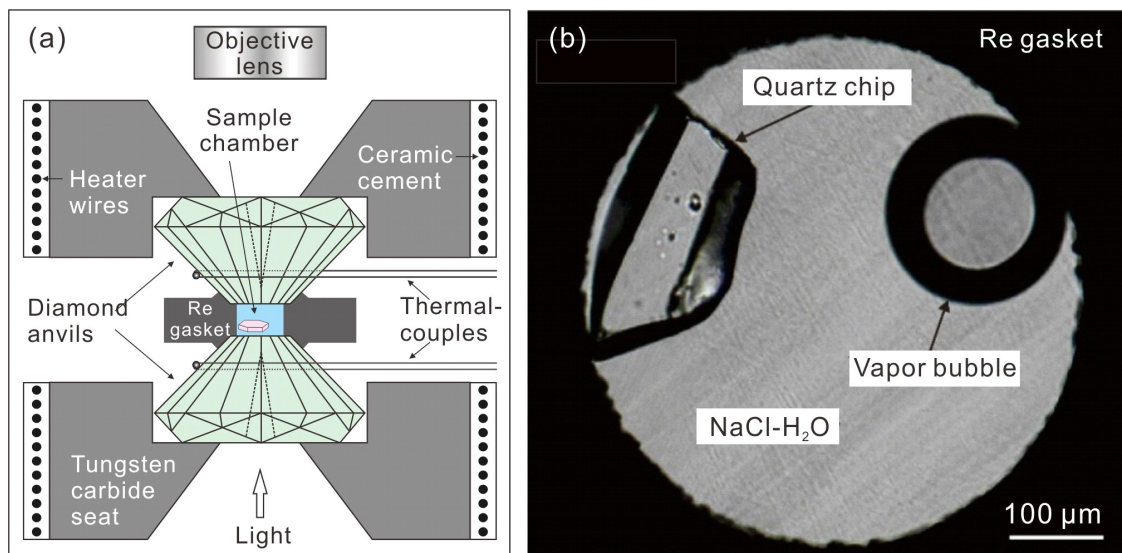


**Figure S-2 (a)** A schematic diagram of the central portion of a hydrothermal diamond-anvil cell (HDAC) and **(b)** the sample chamber loaded with quartz wafer and NaCl-H$_2$O solution (after Bassett *et al.*, 1993; *Li et al.*, 2016)
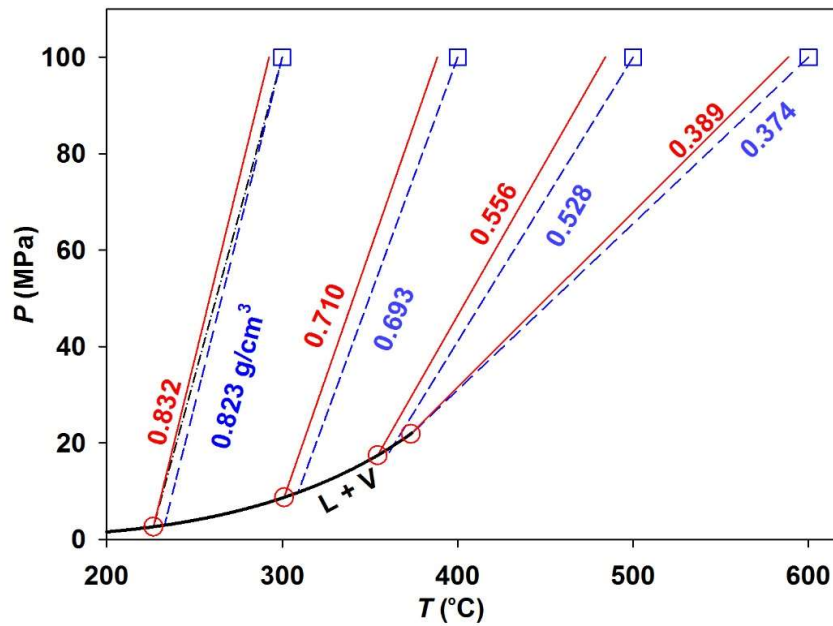
**Figure S-3** $P-T$ (isoplethal) projection showing isochores (g/cm$^3$) of pure $H_2O$ derived from the synthetic fluid inclusion technique data (Bodnar and Sterner, 1987, their Table 17.1) for inclusions formed under 100 MPa. The four blue open squares are the formation $P-T$ points (at 100 MPa and 300, 400, 500 and 600 ºC) of fluid inclusions in quartz, and the corresponding isochores derived from the NIST Table (Wagner and Pruß, 2002) are shown by the dashed blue lines, which end at the liquid-vapor curve (solid black line). The four open red circles on the liquid-vapor curve are the corresponding average liquid-vapor homogenization (to liquid) $P-T$ points of fluid inclusions, and their corresponding isochores are shown by the solid red lines. It is clearly shown that the density represented by the isochoric red line is always higher than that of the corresponding dashed blue line, and that the lines connecting the open red circle and the corresponding blue square (*e.g.,* the black dash-dot line for inclusions formed at 100 MPa and 300 ºC) are not isochoric.
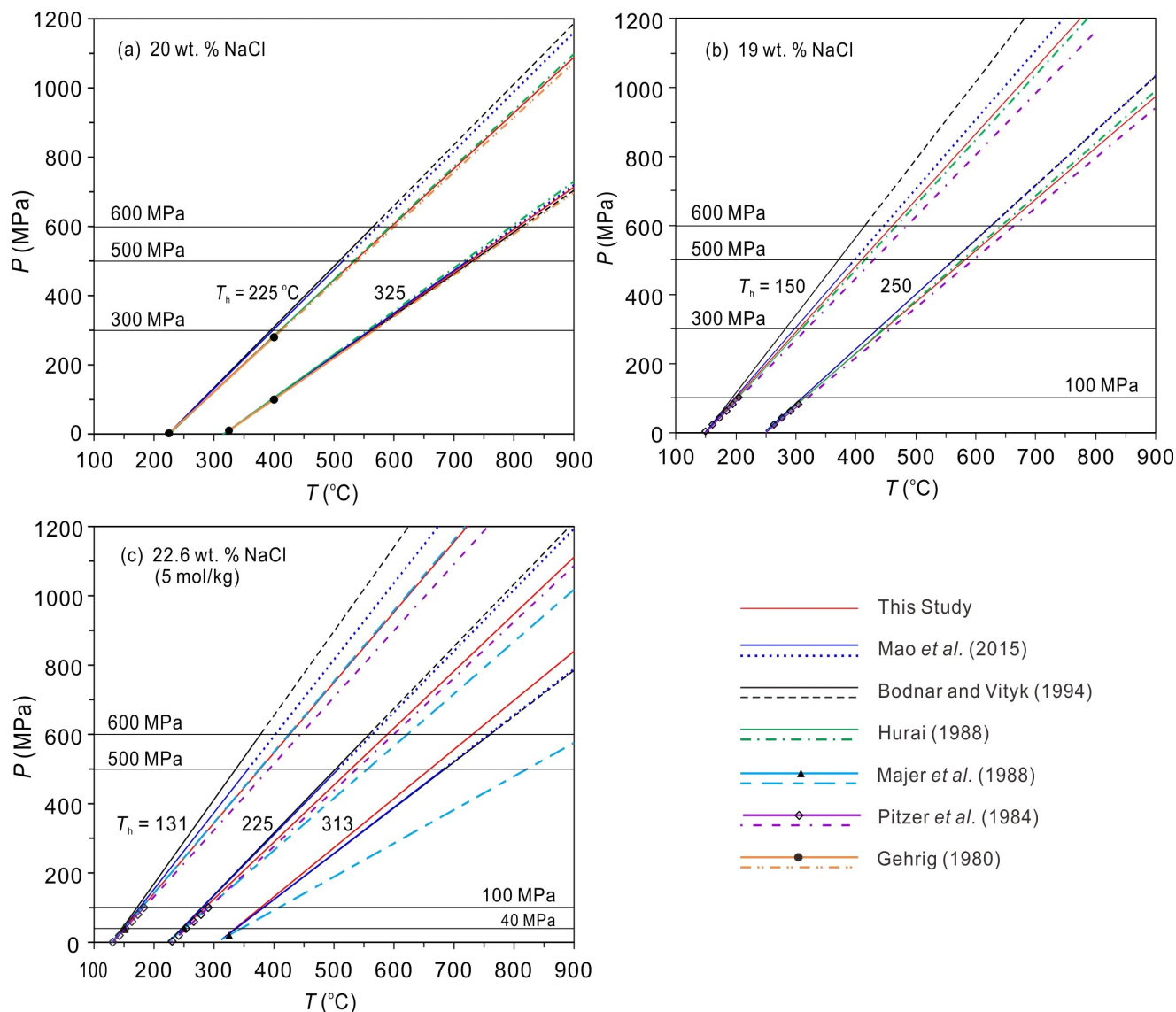
**Figure S-4** Comparisons of NaCl-H$_2$O isochores derived from our data (red lines) and previous ones with **(a)** 20 wt. % NaCl, **(b)** 19 wt. % NaCl, and **(c)** 22.6 wt. % NaCl. The previous isochores include those from Bodnar and Vityk (1994; applicable at ≤600 MPa), Mao *et al.* (2015; applicable at ≤500 MPa), and those linearly fitted with the data in tables of Majer *et al.* (1988; triangle, applicable at ≤40 MPa), Hurai (1988; applicable at ≤500 MPa and 500 °C), Pitzer *et al.* (1984; diamond, applicable at ≤100 MPa), and Gehrig (1980; circle, applicable at ≤300 MPa). All data are represented by solid lines, and extrapolations are shown by other line symbols as indicated in the figure legends at the lower right corner. The homogenization temperatures ($T_h$s) are marked.

# Supplementary Information References

Bassett, W.A., Shen, A.H., Bucknum, M., Chou, I−M. (1993) A new diamond anvil cell for hydrothermal studies to 2.5 GPa and from –190 to 1200 °C. *Review of scientific instruments* 64, 2340–2345. https://doi.org/10.1063/1.1143931

Bodnar, R.J. (1983) A method of calculating fluid inclusion volumes based on vapor bubble diameters and *P-V-T-X* properties of inclusion fluids. *Economic Geology* 78, 535–542. https://doi.org/10.2113/gsecongeo.78.3.535

Bodnar, R.J. (1993) Revised equation and table for determining the freezing point depression of NaCl-$H_2O$ solutions. *Geochimica et Cosmochimica Acta* 57, 683–684. https://doi.org/10.1016/0016-7037(93)90378-A

Bodnar, R.J., Sterner, S.M. (1987) Synthetic fluid inclusions. In: Ulmer, G.C., Barnes, H.L. (Eds.) *Hydrothermal Experimental Techniques*, Wiley-Interscience, New York. 423–457.

Bodnar, R.J., Vityk, M.O. (1994) Interpretation of Microthermometric data for $H_2O$-NaCl fluid inclusions. In: Vivo, B.D., Frezzoti, M.L. (Eds.) *Fluid Inclusions in Minerals: Methods and Applications*. Virginia Tech., Blacksburg, VA. 117–130.

Hurai, V. (1988) *P–V–T–X* tables of water and 1–25 weight percent NaCl-$H_2O$ solutions to 500 °C and 500 $\times$ $10^5$ Pa. *Acta Geologica et Geographica Universitatis Comenianae* 44, 101–135.

Gerhig, M. (1980) Phasengleichgewichte und PVT-Daten temiirer Mischungen aus Wasser, Kohlendioxid und Natriumchlorid bis 3 kbar und 550°C. Ph.D. dissertation, Universitat Karlsruhe, 109p.

Li, J.K., Chou, I-M. (2016) An occurrence of metastable cristobalite in spodumene-hosted crystal-rich inclusions from Jiajika pegmatite deposit, China. *Journal of Geochemical Exploration* 171, 29–36. https://doi.org/10.1016/j.gexplo.2015.10.012

Li, J.K., Bassett, W.A., Chou, I-M, Ding, X., Li, S.H, Wang, X.Y. (2016) An improved hydrothermal diamond anvil cell. *Review of Scientific Instruments* 87, 053108. https://doi.org/10.1063/1.4947506

Li, J.K., Chou, I. M., Bassett, W.A., Wang, X. (2020) A new type of hydrothermal diamond-anvil cell with cooling system. *Review of Scientific Instruments* 91, 053104. https://doi.org/10.1063/1.5143596

Li, S.H., Chou, I-M. (2022) Refinement of the α-β quartz phase boundary based on in situ Raman spectroscopy measurements in hydrothermal diamond-anvil cell and an evaluated equation of state of pure $H_2O$. *Journal of Raman Spectroscopy* 53, 1471-1482. https://doi.org/10.1002/jrs.6367

Majer, V., Gates, J.A., Inglese, A., Wood, R.H. (1988) Volumetric properties of aqueous NaCl solutions from 0.0025 to 5.0 mol kg1, 323 to 600 K, and 0.1 to 40 MPa. *The Journal of Chemical Thermodynamics* 20, 949–968. https://doi.org/10.1016/0021-9614(88)90224-8

Mao, S., Hu, J., Zhang, Y., Meng, X.L. (2015) A predictive model for the PVTX properties of $CO_2$–$H_2O$–NaCl fluid mixture up to high temperature and high pressure. *Applied Geochemistry* 54, 54–64. https://doi.org/10.1016/j.apgeochem.2015.01.003

Pitzer, K.S., Peiper, J.C., Busey, R.H. (1984) Thermodynamic properties of aqueous sodium chloride solutions. *Journal of Physical and Chemical Reference Data* 13, 1–102. https://doi.org/10.1021/ja01341a002

Wagner, W., Pruβ, A. (2002) The IAPWS formulation 1995 for the thermodynamic properties of ordinary water substance for general and scientific use. *Journal of Physical and Chemical Reference Data* 31, 387–535. https://doi.org/10.1063/1.1461829